J Appl Electrochem (2010) 40:435–444
DOI 10.1007/s10800-009-0014-0

ORIGINAL PAPER

Electroless nickel current collector for 3D-microbatteries

T. Ripenbein · D. Golodnitsky · M. Nathan · E. Peled

Received: 4 May 2009 / Accepted: 25 September 2009 / Published online: 15 October 2009

Abstract An electroless nickel process was used for the preparation of a thin-film current collector for concentric three-dimensional lithium and lithium-ion microbatteries. Ni–P coatings were deposited autocatalytically with the use of nickel sulfamate or nickel sulfate as a source of Ni^{2+} and sodium hypophosphite as a reducing agent. The synergistic effect of sodium acetate and citric acid was found to provide marked improvement in the pH stability of the sulfamate electrolyte. This enabled deposition of a conformal, fine-grained film on the high-aspect-ratio glass capillary and perforated-silicon substrates.

Keywords Electroless nickel · Sulfamate electrolyte · Silicon · 3D-microbattery

1 Introduction

The miniaturization of medical and electronic devices entails sub-mm-footprint primary or secondary micropower sources. Lithium-ion batteries show the highest overall performance, but the power and energy density of these microbatteries in typical thin-film planar configuration are limited to their footprint and, therefore, are insufficient for many electronic and medical applications. In order to increase the power and energy density per battery footprint, it is essential to use three-dimensional (3D) architecture. Several battery configurations have been recently proposed to fit these requirements [1]. 3D-concentric microbatteries (3D-CMB) on silicon and glass capillary microchannel plates (MCP), which are under development in our laboratory, have shown the highest energy gain (a factor of 25) and power gain (a factor of 10) per footprint. The 3D-CMB is built onto a high-aspect-ratio perforated substrate. This substrate consists of 20,000 to 30,000 cylindrical through-holes per cm^2 with complete lithium-ion battery units assembled inside each hole and connected in parallel (Fig. 1). The 3D-CMB is made of several conformal thin films of nanosize materials: a nickel current collector, a MoO_xS_{2-x}, MoO_3, or V_2O_5 cathode, a hybrid polymer electrolyte (HPE) and a lithiated-graphite anode [2, 3]. Nickel has been widely used as a current collector for both negative and positive electrodes in lithium-ion cells. An electroless Ni–P alloy deposit was found to be more stable than pure nickel even for high-voltage cathodes (>3.8 V). The fabrication of a high-quality nickel current collector inside deep (500-μm long) and narrow (50-μm diameter) microchannels is one of the key challenges to obtain good performance of 3D concentric microbatteries.

Electroless deposition has undergone a renaissance in recent years, because it is a low-cost, yet versatile route to an even, selective coating of metals on complex-shaped substrates. Over the past several years, electroless deposition has been widely used in the electronic and semiconductor-device industries for producing semiconductor junctions, making ohmic contact, filling vias, and patterning printed-circuit boards [4–9]. The greatest advantage of an electroless process is its ability to plate a non-conductive surface. The main

T. Ripenbein · D. Golodnitsky (✉) · E. Peled
School of Chemistry, Tel Aviv University, 69978 Tel Aviv, Israel
e-mail: golod@post.tau.ac.il

D. Golodnitsky
Wolfson Applied Materials Research Center, Tel Aviv University, 69978 Tel Aviv, Israel

T. Ripenbein · M. Nathan
Department of Physical Electronics, Tel Aviv University, 69978 Tel Aviv, Israel

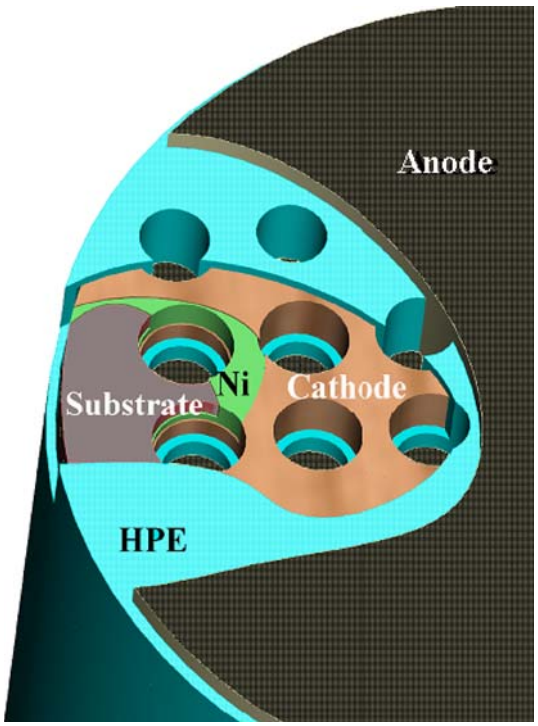

Fig. 1 Scheme of 3D-CMB on perforated substrate

difference between metallic and nonmetallic surfaces is the nature of the bond between substrate and coating. While adhesion to metal is on an atomic level, adhesion to non-conductive substrates is micromechanical. Poor surface preparation is followed by lack of adhesion, deposit porosity, high roughness, non-uniform coatings, and dark deposits, all of which cause deterioration in the quality of the battery layers and, as a result, in the energy and power characteristics of the 3D-CMB. In the worse case, poor adhesion of the nickel current collector to the substrate may cause short-circuits in the battery. There are numerous studies of electroless nickel deposits with high- and low-phosphorus content on silicon substrates [10–18]. However, as far as we know, no results of investigations on the growth morphology, crystallinity, and composition of electroless Ni–P deposits on 3D-Si and 3D-glass high-aspect-ratio substrates have been published.

In this study, our main concern has been with the effect of electrolyte composition and operating conditions on the morphology and uniformity of electroless nickel coatings on 3D-substrates. Also treated at some length is the development of efficient surface-pretreatment procedures for 3D perforated-silicon wafers and MCPs in order to achieve high Ni–Si and Ni–glass adhesion.

2 Experimental

A silicon substrate containing arrays of through-holes was prepared with the use of photolithography and double-sided Deep Reactive-Ion Etching (DRIE). The (100) substrate was a double-side polished, 440 μm-thick, 4 inch silicon wafer. The wafer was coated with about 10 μm of AZ-4562 photoresist, and arrays of square holes with a side dimension of 40 μm and inter-hole spacing of about 10 μm were defined. Soda-lime glass is the most common and cheapest commercial glass. The composition of soda-lime glass is normally 60–75% SiO_2, 12–18% Na_2CO_3, and 5–12% CaO–MgO. The ductility of soda-lime glass at elevated temperatures allows the formation of precision glass capillary tubes, which produce a uniform and mechanically rigid structure when fused together. Such structures, thinly sliced, can serve as substrates for the 3D concentric microbattery. These glass capillary arrays (GCAs) (i.e., MCPs) are sold by *Burle Industries Inc*. (http://www.burle.com/index.html). *Mikroglas Chemtech GmbH* sells Foturan (http://cnd.vscht.cz/projects/foturan.html), lithium–aluminum–silicate photosensitive glass, which enables patterning for a variety of purposes.

All deposition experiments were performed in aqueous solution, with water of 18 MΩ cm resistivity (Millipore, Watford, UK). Analytical-grade reagents (Sigma–Aldrich) were used for the preparation of etching solutions and nickel electrolytes.

Foturan and soda-lime glass 2D and 3D samples were degreased and etched in the solutions, the compositions of which are shown in Table 1.

Prior to being coated with nickel, the substrates were subjected to sensitization and activation procedures. Sensitization was carried out in a solution containing 20–50 g L^{-1} $SnCl_2{\cdot}H_2O$; 40–50 mL L^{-1} HCl (32%). In the case of glass substrates, ethanol was added to the solution in order to improve adsorption of Sn^{2+} ions. The activation bath contained 0.5–1.5 g L^{-1} $PdCl_2$; 1.5–10 mL L^{-1} HCl (32%).

Silicon substrates, before activation in Pd-containing solution, were treated in the solutions listed in Table 2. In order to ensure homogeneous coating of silicon by a thin palladium layer, HF (40%) was added to the sensitization solution.

Two electroless nickel-plating baths were used for coating the substrates and for adhesion tests (Table 3).

A sulfate-based electrolyte was used for coating silicon and Foturan. A sulfamate-based electrolyte was developed for glass capillary arrays, but it was tested on silicon as well.

Adhesion was examined with the help of adhesive tape. A JSM-6300 scanning microscope (Jeol Co.) equipped with a Link elemental analyzer and a silicon detector was used to study surface morphology. X-ray-diffraction data were obtained with the use of a θ–θ Scintag powder diffractometer equipped with a Cu Kα source and a liquid-nitrogen germanium solid-state detector.

Table 1 Surface pretreatment steps of planar and 3D Foturan and glass substrates

Procedure	No.	Constituents	Composition (v/v) and operating conditions
Degreasing	1	Ethanol	
	2	Acetone	
	3	Cyclohexane	80 °C
	4	Detergent	RT
Etching	1	Solution of chromo-sulfuric acid in water (95% H_2SO_4; <2% CrO_3)	1:4
	2	HF (40%):H_2SO_4 (98%)	1:4
	3	HF (0.8 M) and NH_4F (0.5 M)	
	4	NaOH (10 M)	
	5	HNO_3 (69%):H_2SO_4 (98%)	1:1
	6	H_2SO_4 (98%)	
	7	CH_3OH:HCl (32%)	1:1
	8	H_2SO_4 (98%):H_2O_2 (30%) (Piranha solution)	3:1

Table 2 Solutions for etching of silicon samples

No.	Constituents	Composition (v/v)
1	HF (40%):HNO_3 (69%)	1:9
2	HF (40%):HNO_3 (69%):H_2O	2:5:4
3	HF (40%):HNO_3 (69%):CH_3COOH (glacial)	4:7:4
4	HF (40%):HNO_3 (69%):CH_3COOH (glacial)	2:15:5
5	HF (40%):HNO_3 (69%):CH_3COOH (glacial)	7:4:4
6	HF (40%):CH_3CH_2OH (abs):H_2O_2 (30%)	1:1:1
7	HF (40%):CH_3CH_2OH (abs):H_2O_2 (30%)	1:1:2

3 Results and discussion

3.1 Surface pretreatment of 3D-substrates

Before carrying out electroless nickel deposition, perforated-Foturan samples were cleaned either in acetone and then in ethanol, or in cyclohexane followed by immersion in a solution of chromo-sulfuric acid (see Sect. 2). The latter pretreatment procedure was found to be more effective.

The purchased Foturan samples have significantly different roughness levels inside the channels and on the planar surface. The latter is polished, while the inner surface of the channels is ground and has irregularities up to

Table 3 Compositions of the Ni electroless baths for adhesion tests

Constituents of the bath (g L^{-1})	Concentration	
	Bath I	Bath II
$NiSO_4 \cdot 6H_2O$ (Nickel sulfate)	20–40	
Ni $(SO_3NH_2)_2 \cdot H_2O$ (Nickel sulfamate)		15–30
$Na_3C_6H_5O_7 \cdot 2H_2O$ (Sodium citrate);	30–90	30–90
CH_3COONa (Sodium acetate)		10–20
CH_4N_2S (Thiourea)		0.05–0.2
$C_7H_5NO_3S$ (Saccharin)		0.01–0.03
$CH_3(CH_2)_{11}OSO_3Na$ (Sodium lauryl sulfate)		0.005–0.02
$NaPO_2H_2$ H_2O (Sodium hypophosphite)	10–40	10–40
NH_4OH (25%)	The amount needed to obtain the desirable pH value	
Operating conditions		
pH	6–9	9–9.5
Temperature (°C)	70–80	60–90
Plating time (min)	5–10	5–10

15–20 μm in size. The dissimilar roughness could result in differences in the adhesion of the deposit. This, in turn, could lead to peeling of the metal film from the planar surface or to the creation of microneedles inside the channels, which could tear the thin-film membrane and cause short-circuits, degrading the performance of the whole microbattery. In order to increase the roughness level of the polished Foturan glass surface, and simultaneously polish the inner surface of the channels, the samples were treated with several etching solutions (Table 1). The treatment of the sample with the first three solutions did not improve the roughness level of the planar surface and the adhesion of the nickel deposit was poor. Immersion of Foturan substrates in a hot (80 °C) concentrated solution of NaOH (solution 4 in Table 1) for 2.5 h resulted in homogeneous etching of the surface and a roughness level of 0.4 μm. The strongest adhesion of nickel to the planar part of the Foturan samples was obtained by a sand-blast-abrasion method.

The second candidate tested for application as a substrate in 3DCMBs was a multichannel plate consisting of glass capillary arrays. Figure 2 shows the SEM images of the planar and cross-sectional view of a sample. The differences in the roughness levels of the planar and the inner surfaces of the capillary are those found in the commercial samples of the MCPs. The electroless nickel deposit adheres well and is homogeneous after the sample is etched for 10 s in a solution of 4 M HF, 8 M H_2SO_4.

None of the etching solutions listed in Table 2 was efficient for the preparation of nickel layers that were highly adhesive to 3D silicon. As with the Foturan and MCP substrates, after ICP perforation, the silicon wafers showed a significant difference between the surface morphology inside a microchannel and that of a flat area. Even after etching in solutions 1–5, the flat area is rather smooth, with a mean roughness of about 10 nm. The roughness inside a microchannel varies from 16 to 100 nm. With the aim of achieving uniform roughness of the silicon substrate, we attempted to modify the method of metal-assisted etching [19]. This is a two-step procedure which includes electroless coating of silicon with numerous sub-micron-size islands of a noble metal, followed by etching in a solution containing HF, oxidizing agents, and other additives. When immersed in a solution containing an ion of a noble metal and hydrofluoric acid, the silicon substrate functions as an internal electron source for spontaneous metal deposition on its surface [20]. Figure 3a and b shows the surface of silicon samples dipped in $PdCl_2$/HF solution for 5 s and then etched for 20 s in two solutions that differ only in the concentration of hydrogen peroxide (solutions 6 and 7 from Table 2). The size of the pits is uniform and their diameters are about 0.3 μm. This roughness level results in very strong adhesion of the electroless nickel deposit to silicon and allows the consideration of silicon as a substrate for 3D microbatteries.

Thermal treatment (400–420 °C for 5 min in an argon atmosphere) of the nickel-coated silicon samples improved adhesion still further. This was due to nickel diffusion into the bulk of the silicon and the formation of a nickel silicide layer about 100 nm thick on the interface between the substrate and nickel, as found by the TOF–SIMS method.

3.2 Deposition of a nickel current collector for 3D-CMBs from a nickel sulfate bath

Figure 4 shows cross-sectional and planar SEM images of the perforated-silicon substrate coated by an electroless nickel layer. The plating was performed at pH 9, 80 °C for 10 min and the thickness of the nickel film was about 3 μm. As can be seen in the figure, a thin, conformal nickel layer completely coats the planar surface and the interior of a channel. The adhesion of the deposit, as detected by adhesive-tape tests, is strong. Some peeling, shown in Fig. 4, is due to the rough mechanical cut of the sample. The AFM image (Fig. 4c) indicates an average roughness level of the nickel film in the range of 0.7–1.5 μm.

In order to determine the optimal plating conditions, the morphology and thickness of the deposit were tested. Figure 5 shows a plot of the thickness of the electroless nickel coating versus deposition time at pH 9 and 80 °C. The thickness of the nickel deposit increases linearly with deposition time, varying from 2 to 12 μm over a time range

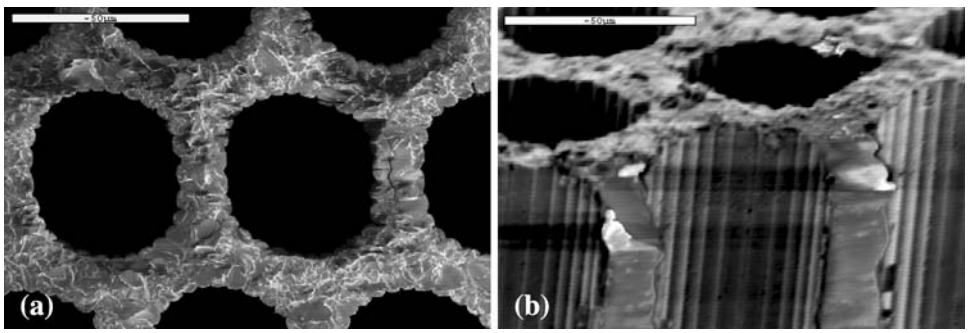

Fig. 2 SEM images of MCP (Burle). **a** The planar view of the surface, **b** the tilted view of a cross-section. *The size bar* indicates 50 μm

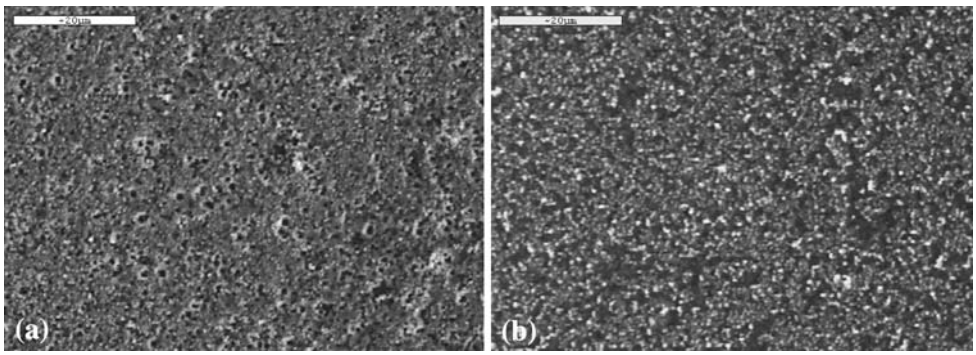

Fig. 3 SEM images of a planar silicon surface treated for 20 s. **a** in solution 6, **c** in solution 7 (Table 2) Scale bar: 20 μm

of 10–35 min. From the experimental data, the estimated deposition rate was 0.39 μm min^{-1}. At lower pH and temperature, the deposition rate decreased sharply and this was reflected in a thinner nickel deposit. At pH 7 and 70 °C, for example, the estimated deposition rate was only 0.07 μm min^{-1}. The grain size of the nickel coating on silicon, as detected by SEM increases from 0.5 to 1.7 μm as the pH rises from 7 to 9. According to [21], when the deposit is thin, the deposition process is characterized by nucleation and growth of three-dimensional crystallites. At longer deposition times, a continuous electroless film is formed by lateral growth and coalescence of crystallites. This is in agreement with the SEM micrographs of nickel deposits (not shown here). The grain size of the nickel deposits varied from 0.3 to 1 μm for a 10-min deposition, and from 1 to 5 μm for a 75-min deposition. On the basis of the experimental results, the optimized nickel sulfate plating bath is composed of: 32 g L^{-1} $NiSO_4 \cdot 6H_2O$; 36 g L^{-1} $Na_3C_6H_5O_7 \cdot 2H_2O$ (sodium citrate); 33 g L^{-1} $NaH_2PO_2 \cdot H_2O$ (sodium hypophosphite); pH 9 (adjusted with NH_4OH (25%)), $T = 80$ °C.

When an attempt was made to use this bath for the coating of glass-capillary MCPs, a very vigorous reaction occurred with strong evolution of hydrogen. The deposition rate became uncontrollable, and this resulted in rapid precipitation of nickel, both on the sample and on the walls and bottom of the plating bath. We explain this by the significant difference between the surface areas of three-dimensional silicon and glass substrates. The geometrical area of the 3D-glass MCP substrates is 23 times that of the

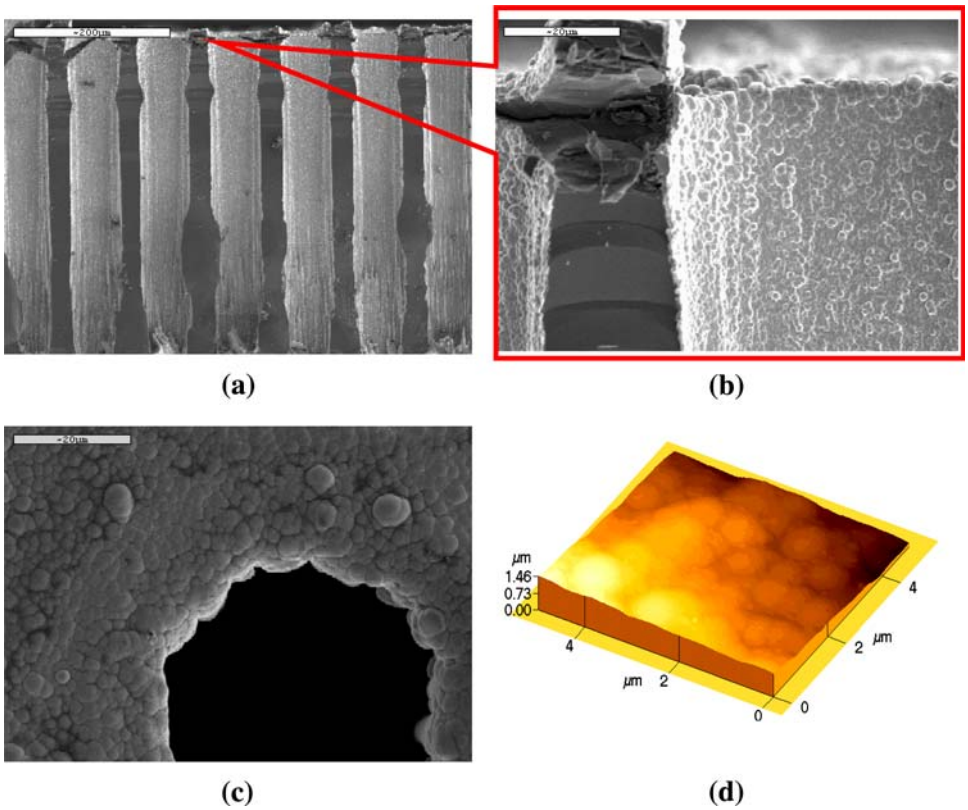

Fig. 4 SEM (**a**–**c**) and AFM (**d**) images of a three-dimensional silicon substrate coated in an electroless nickel sulfate bath. **a** Cross-section of coated channels; *the size bar* indicates 200 μm; **b** Enlarged view of the upper part of the cut sample. *The size bar* indicates 20 μm; **c** Top view of the planar surface of the coated sample. *The size bar* indicates 20 μm; **d** AFM image of Ni current collector

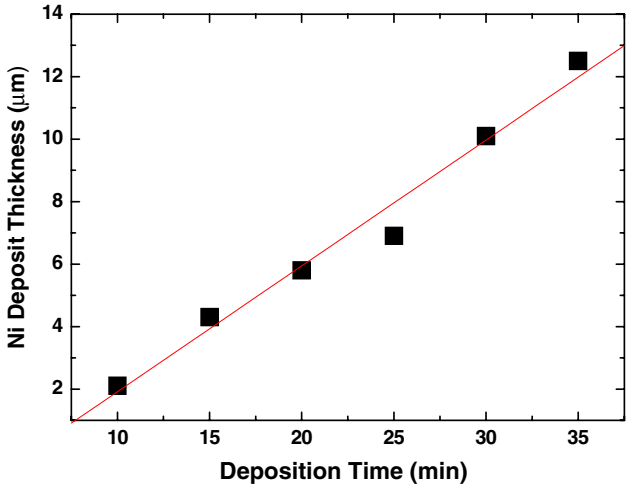

Fig. 5 Thickness of electroless Ni deposit versus deposition time (pH 9, 80 °C)

planar footprint, more than twice the area gain of 3D perforated silicon. This, together with the rough surface of the interior of the glass microchannels, results in a very high surface area for the MCP. As a result of the pore-infiltration property of the plating solutions, metallization takes place on the rough surface of the microchannels over an effective area that is much higher than the geometrical area of the sample. This is followed by a highly inhomogeneous nickel deposit with incomplete coverage of the internal surface of the microchannels and a thick deposit on the planar surface. As mentioned above, defects in the nickel deposit along the channel would cause poor electrical contact, which could impede the subsequent electrodeposition of the cathode layer and cause malfunction of the whole cell. In addition, inside a channel, just near its opening, large agglomerates are formed (SEM images are not shown here). These could go through all the successive microbattery layers and cause a short circuit. We tried to change the pH, temperature, and concentration of complexing agent in the sulfate bath, but variation of these parameters caused destabilization of the plating process and change in the morphology of the deposit.

3.3 Deposition of a nickel current collector for 3D-CMBs from a nickel sulfamate bath

In general, the nickel sulfamate bath is widely used in electrodeposition or electroforming because of its advantages, such as the high solubility of sulfamate salts in aqueous solution, which enables high-current–density applications, and stability greater than that of sulfates. This electrolyte is known to have good throwing power and the ability to form thick films with low tensile stresses. It has recently been shown that there is either no formation of nickel sulfamate complexes in the bulk of the electrolyte or that any complexes formed are weak and unstable [22]. As in the case of sulfate electrolytes, electro- and electroless deposition of iron-group metals from sulfamate electrolytes are followed by a local pH rise near the electrode surface (pH_s). In the absence of buffering agents, even in acidic electrolytes, there is surface precipitation and occlusion of hydroxides, which are detrimental to the growing deposit. In alkaline media, the operating solution becomes turbid as a result of the formation of basic nickel-salt hydroxides. However, contrary to the case of sulfate solutions, in sulfamate electrolytes at temperatures higher than 60 °C, nickel sulfamate hydrolyses and ammonium ions are released. While the high-temperature hydrolysis makes the sulfamate electroless nickel bath more stable as a result of the formation of $Ni(NH_3)_x^{2+}$ complexes, the presence of complexing, buffering, and stabilizing agents is still essential.

We have found that in sulfamate solutions containing no thiourea, there is a random, spontaneous reduction of nickel on the high-aspect-ratio MCP. This is followed by complete decomposition of the electrolyte. Bath decomposition is usually preceded by an increase in the volume of hydrogen gas evolved and the appearance of fine black particles in the bulk of the solution. The precipitate consists of nickel particles and nickel phosphide. The addition of a stabilizer like thiourea prevented the reaction that triggers the subsequent random decomposition of the entire plating bath. According to [23], the rate of nickel electroless deposition on the surface increases as a result of the transfer of electrons from thiourea to the nickel ions, yielding elemental nickel and a dimer of thiourea. The dimer is then reduced by the transfer of electrons from hypophosphite to form thiourea again. However, increasing the concentration of thiourea above 0.2 mg L^{-1} completely inhibits the plating reaction. We also found that saccharin inhibits the coalescence of electroless nickel nodules, and sodium dodecylsulfate eliminates the formation of pitting in the deposit.

Figure 6 depicts the SEM images of electroless nickel deposited on a 3D-MCP substrate in a modified sulfamate solution that contains citrate and acetate complexing agents. It can be seen that the nickel coating follows the surface morphology of the microchannels and completely covers the interior of the glass capillary tube. The electroless Ni–P deposits from the sulfamate bath were uniform, semi-bright in appearance, and comprise spheroids of different sizes. Because of their nodular surface characteristics, the deposits typically exhibited a rough profile. The thickness of the film is about 1.5 μm when the electroless process is carried out for 10 min at pH 9 and 70 °C.

Figure 7 shows the influence of pH on the grain size of nickel. At pH 8 (Fig. 7a), the nickel deposit is thin (about

0.4 μm after 5 min of deposition); its surface is relatively smooth, since the kinetics of nucleation is faster than the rate of crystal growth. The spheroids are already noticeable at this thickness. At pH 9 (Fig. 7b), the reduction of nickel by hypophosphite is faster and crystal growth becomes more significant. At pH 10, the deposition rate increases further (Fig. 7c), leading to greater thickness (up to an average of 1.2 μm) and larger spheroids, the size of which approaches 1 μm. The electroless nickel coating becomes highly non-homogeneous with compact agglomerates at the top of the concave, finned part of the internal surface of the microchannel.

High temperature accelerates the process, affecting mainly the thickness of the coating, which increases from ~0.6 to 1 μm at 60 and 70 °C, respectively. While somewhat larger ball-like particles appear at the surface, the uniformity of nickel plating as well as the roughness factor does not change much with temperature. The deposit conformally follows both the internal 3D and planar surfaces of the MCP.

Figures 8 and 9 show the effect of the concentrations of reducing and complexing agents in the electroless-nickel bath on the morphology of nickel and the deposition rate. Lowering the concentration of the sodium hypophosphite leads to a decrease in the reaction rate, and thus, to a reduction in the thickness of the deposit and the dimensions of the spheroids. The average thickness of the nickel film formed in a solution containing 16.6 g L^{-1} NaH_2PO_2 is less than half that obtained from the electrolyte with 33.3 g L^{-1} of reducing agent. Rapid reduction of Ni^{2+} at high concentrations of hypophosphite causes vigorous growth of spheroid particles on top of the convex ribs, while the deposit on the concave parts between the ribs is much thinner. This causes highly non-uniform nickel films in the microchannels.

Citrate has the opposite effect on the deposit. Here, increasing the sodium citrate concentration in the electrolyte leads to a reduction in the thickness of the deposit and the radius of the spheroids (Fig. 9). For a deposition time of 5 min, the thickness of the nickel deposit decreases almost linearly from 0.95 to 0.2 μm as the concentration of sodium citrate is increased from 22.1 to 73.5 g L^{-1}. SEM images of the MCP coated by nickel (Fig. 9) show that increasing the concentration of sodium citrate results in the formation of a uniform deposit with a smooth, homogeneous surface.

In agreement with [24], we believe that at pH > 8, citrate forms $NiHCit^{-}$, $Ni_2Cit(HCit)^{3-}$, and $Ni_2Cit_2^{4-}$ complexes which, in turn, prevent the formation of the undesirable nickel hydroxide inclusions and detrimental roughness of the plating. The presence of acetate, although a weaker complexing agent than citrate, increases the buffer capacity of the electrolyte.

The rate of electroless nickel deposition and the phosphorus content are proportional to the rate at which the nickel complex dissociates to form free nickel ion. Thus, the plating rate is inversely related to the stability of the nickel complexes. The deposition rate of nickel obtained from a modified sulfamate bath at pH 9 and 70 °C was 0.207 μm min^{-1}. This deposition rate is lower than the rate in a nickel sulfate bath, but the deposit is much more uniform in thickness, conformal with a smoother surface and smaller grain size (Fig. 10). It should be noted, in addition, that both the roughness and the uniformity of nickel obtained from a dual-modified sulfamate electrolyte do not change much with time. The concentration of phosphorus in a Ni–P alloy obtained by EDS measurements is only slightly affected by the deposition time. The phosphorus content increases by 1.5% when the duration of the reduction process is increased from 2 to 10 min. When the thickness of the nickel layer approaches 1.5 μm, the Ni–P deposit contains 14.2% phosphorus. This composition remains unchanged up to a film thickness of 4 μm. Structural examination carried out by XRD revealed the presence of a broad peak with a calculated crystallite size of about 1.5 nm for nickel deposited from a modified sulfamate electrolyte, whereas a sharp (111) peak with a crystallite size of about 6 nm is obtained for the metal from a sulfate bath. A small, broad shoulder appearing at

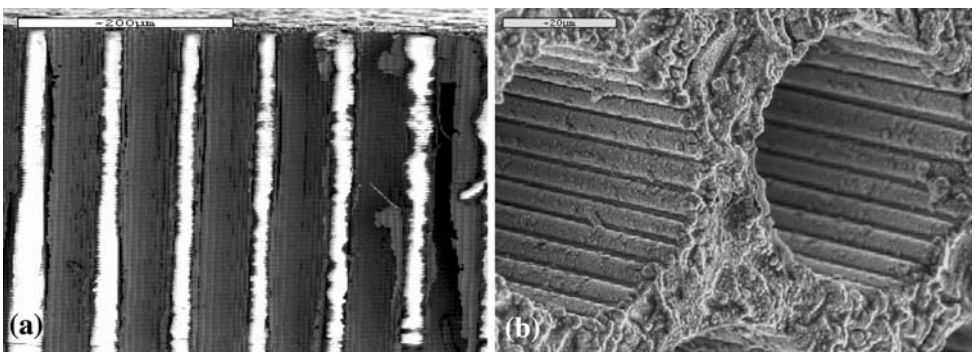

Fig. 6 SEM images of MCP coated in an electroless nickel sulfamate bath at pH 9, 70 °C, 10 min; **a** Cross-section of coated channels; *the size bar* indicates 200 μm; **b** Tilted view of the surface of the coated sample. *The size bar* indicates 20 μm

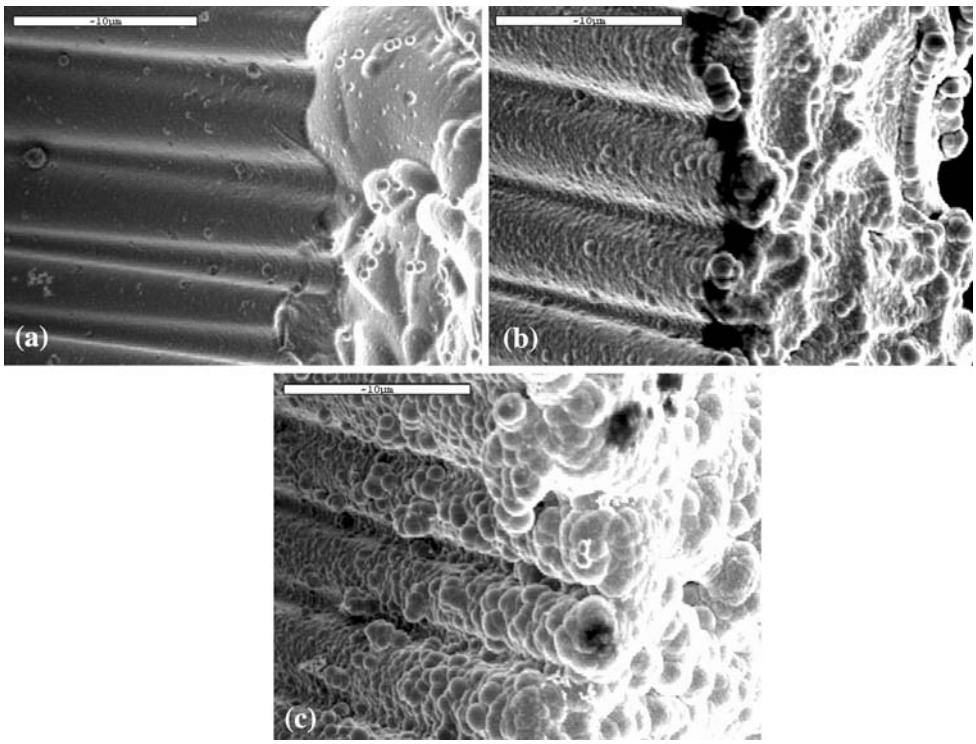

Fig. 7 SEM images of tilted MCP surface coated at $T = 70^{o}$ C for 5 min **a** pH 8; **b** pH 9; **c** pH 10. *The size bar* indicates 10 μm

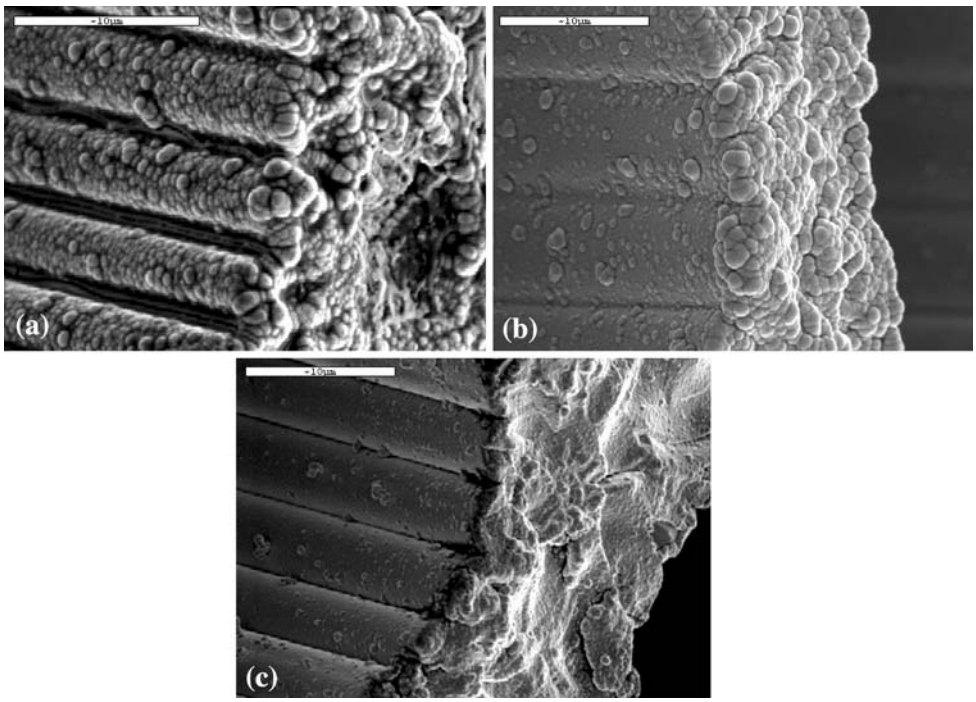

Fig. 8 SEM images of tilted MCP surface coated at different concentrations of Na-hypophosphite, g L^{-1}: **a** 33.3; **b** 25.4; **c** 16.6. *The size bar* indicates 10 μm. Time of deposition—5 min

48° in the latter XRD pattern (not shown here) can possibly be attributed to some amorphous inclusions, like nickel hydroxide and nickel phosphide in the deposit. The average roughness factor of the Ni–P films deposited on the glass and silicon substrates and determined by the AFM tests is 1–1.3 and 0.8–1.0 μm, for the samples obtained from the sulfate and modified sulfamate solutions, respectively.

As a current collector for a microbattery, the nickel electroless deposit has to provide high electrical conductivity. The resistivity of the 3D nickel layer, deposited at pH 9, for 5 min at 70 °C, measured by the AC-impedance

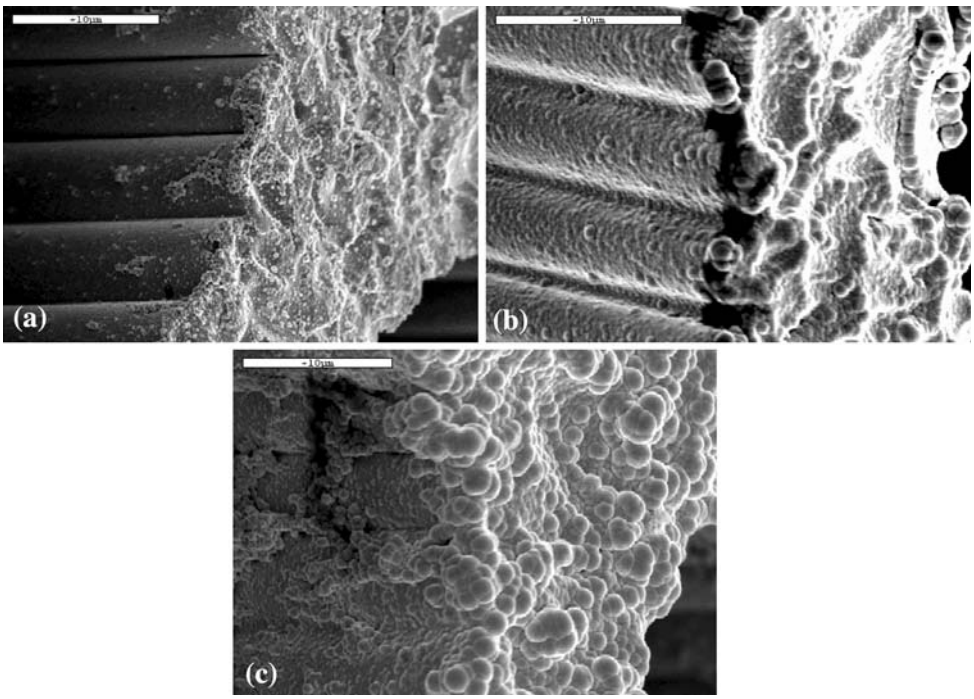

Fig. 9 SEM images of tilted MCP surface coated at different concentrations of Na citrate, g L^{-1}: **a** 73.5; **b** 36.6; **c** 22.1. *The size bar* indicates 10 μm. Time of deposition—5 min

method, was 102 μΩ cm. This value is in agreement with the theoretical value of the resistivity for nickel deposits with high phosphorus content. Such conductivity is quite sufficient for a battery current collector.

The optimal conditions for the deposition of a conformal 1–1.5 μm-thick-film nickel current collector to be used in the 3D concentric microbatteries are as follows: 18 g L^{-1} $Ni(SO_3NH_2)_2{\cdot}H_2O$ (nickel sulfamate); 36 g L^{-1} $Na_3C_6H_5O_7{\cdot}2H_2O$ (sodium citrate); 14 g L^{-1} CH_3COONa (sodium acetate); 33 g L^{-1} $NaH_2PO_2{\cdot}H_2O$ (sodium hypophosphite); 0.1 mg L^{-1} CH_4N_2S (thiourea); 25 mg L^{-1} saccharin; 10 mg L^{-1} $CH_3(CH_2)_{11}OSO_3Na$ (sodium dodecylsulfate); pH 9 (adjusted with NH_4OH (25%)); $T = 70$ °C; Deposition time = 5–7 min.

4 Conclusions

Two electrolytes have been tested for the deposition of thin-film nickel on the three-dimensional perforated silicon and microchannel glass substrates. The deposits were characterized as to their structure, morphology, crystallization behavior, and composition.

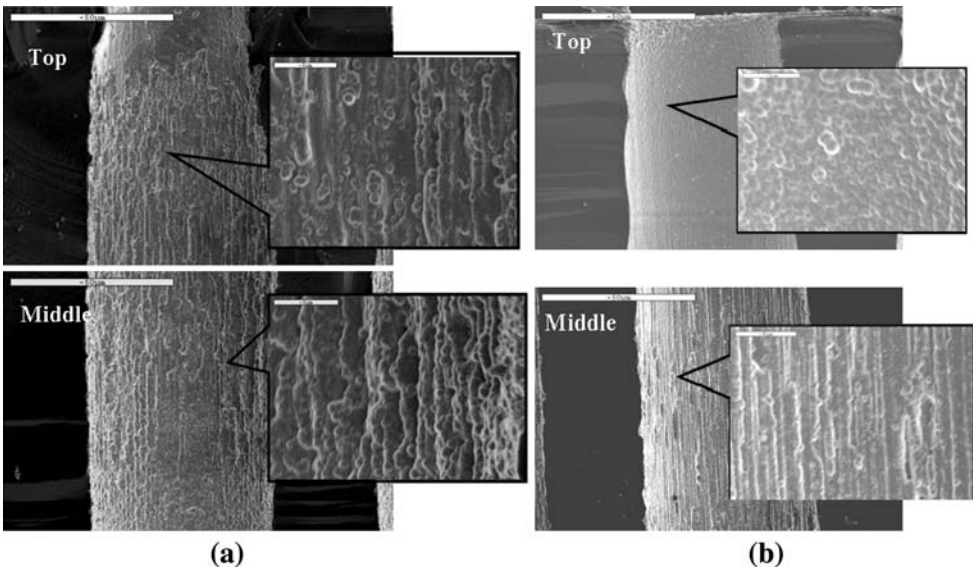

Fig. 10 Cross-sectional SEM images of non-polished perforated-Si substrate coated by Ni from sulfate (**a**) and modified sulfamate (**b**) electrolytes. *The scale bars* indicate 50 and 5 μm on the insets

A sulfamate-based electrolyte with double complexing-buffering agents enabled the deposition of an electroless nickel layer of homogeneous morphology and composition at a controllable reduction rate.

While high citrate content in the electrolyte improves the morphology and uniformity of the nickel layer on complex 3D substrates with high-aspect-ratio microchannels, increase of the molar ratio between Ni^{2+} and citrate above 1:1 is followed by a significant drop in the reduction rate, which seems impractical for industrial applications.

Thiourea was added to the solution to prevent the vigorous reaction on the high surface area glass capillary plates that triggers the subsequent random decomposition of the entire plating bath.

Additions of saccharin and sodium dodecylsulfate eliminated the formation of pitting in the deposit and improved its adhesion to the substrate.

Results obtained from EDX analysis showed that the binary Ni–P alloy deposited from a dual-modified sulfamate electrolyte contains 12–14% phosphorus. The coating was composed of about 1.5 nm-size crystallites.

Acknowledgments We express our gratitude to RAMOT (University Authority for Applied Research and Industrial Development Ltd.) and to the European Community ("Superlion" project) for the partial support of this research.

References

1. Long JW, Dunn B, Rolisson D, White H (2004) Chem Rev 104:4463
2. Nathan M, Golodnitsky D, Yufit V, Strauss E, Ripenbein T, Shechtman I, Menkin S, Peled E (2005) J MEMs 14(5):879
3. Golodnitsky D, Yufit V, Nathan M, Shechtman I, Ripenbein T, Strauss E, Menkin S, Peled E (2006) J Power Sour 153:281
4. Cachet H, Froment M, Souteyrand E (1992) J Electrochem Soc 139:2920
5. Ting CH, Paunovic M, Pai PL, Chiu G (1989) J Electrochem Soc 136:462
6. Kennedy RM, Minten K, Yang X, Evans DF (1991) J Vac Sci Technol B 9:735
7. Tsai T-K, Chao C-G (2004) Appl Surf Sci 233:180
8. Seo MH, Kim JS, Hwang WS, Kim DJ, Hwang SS, Chun BS (2004) Surf Coat Technol 176:135
9. Shacham-Diamad Y, Sverdlov Y (2000) Microelectron Eng 50:525
10. Lynch JE, Pehrsson PE, Leonard DN, Calvert JM (1997) J Electrochem Soc 144:1698
11. Rohan JF, O'Riordan G, Boardman J (2002) Appl Surf Sci 185:289
12. Lin KL, Chen CL (2000) J Electrochem Soc 147:2604
13. Wang J, Fei X, Yu Z, Zhao G (1995) Appl Surf Sci 84:383
14. Korda′s K, Remes J, Leppavuori S (2001) Appl Surf Sci 178:93
15. Niwa D, Takano N, Yamada T, Osaka T (2003) Electrochim Acta 48:1295
16. Harris TM, Dang QD (1993) J Electrochem Soc 140:81
17. Saitou M, Okudaira Y, Oshikawa W (2003) J Electrochem Soc 150:140
18. Zeller RL III, Landau U (1992) J Electrochem Soc 139:464
19. Li X, Bohn PW (2000) Appl Phys Lett 77(16):2572–2574
20. Arunagiri T, Golden TD, Chyan O (2005) Mater Chem Phys 92:152
21. Paunovic M, Schlesinger M (1998) Fundamentals of electrochemical deposition. Wiley, New York
22. Golodnitsky D, Gudin N, Volyanyuk G (1998) Plat Surf Finish 2:65–73
23. Mallory GO (1991) In: Mallory GO, Hajdu J (eds) Electroless plating: fundamentals and applications. Noyes Publications/William Andrew Publishing, Norwich, p 1
24. Golodnitsky D, Gudin NV, Volyanuk GA (2000) J Electrochem Soc 147(11):4156–4163